Structure and electrical properties of nanoparticulate tungsten oxide prepared by microwave plasma synthesis

M Sagmeister[1], M Postl[2,3], U Brossmann[1], E J W List[2,3], A Klug[3], I Letofsky-Papst[4], D V Szabó[5] and R Würschum[1]

[1] Institute of Materials Physics, Graz University of Technology, Petersgasse 16, A-8010 Graz, Austria
[2] Institute of Solid State Physics, Graz University of Technology, Petersgasse 16, A-8010 Graz, Austria
[3] NanoTecCenter Weiz Forschungsgesellschaft GmbH, Franz-Pichler-Straße 32, A-8160 Weiz, Austria
[4] Institute for Electron Microscopy and Fine Structure Research, Graz University of Technology, Steyrergasse 17, A-8010 Graz, Austria
[5] Institute for Materials Research III, Karlsruhe Institute of Technology, D-76021 Karlsruhe, Germany

E-mail: brossmann@tugraz.at

Abstract
Nanoparticulate WO_3 films were prepared using microwave plasma synthesis and studied with respect to the electrical conductivity in dependence of ambient conditions. The WO_3 films with a monoclinic structure were made from cluster-assembled nanoparticles (diameter 3 nm) by means of dispersion and spin-coating. Above 100 °C a thermally activated decrease of the electrical resistance due to oxygen vacancy donors is found. A reversible increase of the electrical resistance R due to oxygen uptake is observed. The decrease of R in response to reducing H_2S in the ppm range is studied in dependence of temperature and pre-annealing conditions.

1. Introduction

Nanostructured materials with novel properties and potential applications arising from the large fraction of atoms at interfaces are the focus of intense studies both with a view to basic research and the development of technical applications, see Vollath [1] for a review. Nanocrystalline transition metal oxides, such as ZrO_2, WO_3 and SnO_2, constitute a particularly interesting class of materials [2–4]. Their structural properties and electrical conductivity are governed by the grain size and small deviations from stoichiometry [5]. The latter sensitively depends on doping with cations of different valence as well as on ambient conditions, such as humidity and the partial pressure of oxygen [6]. Furthermore, studies in the literature show that the variation of the electrical conductivity of tungsten oxide can be used to detect small concentrations in the ppm range of both oxidizing gases, such as NO_x, and reducing gases such as H_2S and NH_3, giving it a high potential for use in gas sensor devices [4, 7–9]. The dependence of all these properties on the grain size [5, 10] provides a motivation for the present studies on nanoparticulate WO_3 prepared by microwave plasma processing.

Microwave plasma synthesis constitutes a powerful and versatile technique for obtaining a wide range of such nanoparticulate oxide materials with a small grain size and narrow size distribution [11]. Volatile metal–organic or carbonyl precursors are decomposed in a non-equilibrium plasma at temperatures typically not exceeding 500 °C in the gas stream, which is much lower than in a conventional tubular furnace or arc discharge [11, 12]. It is therefore possible to fabricate mixed oxide (e.g. $Y_2O_3{\cdot}ZrO_2$) or core–shell particles and—most importantly—to disperse these particles in liquids for subsequent processing steps, such as spin-coating and ink-jet printing [11, 13, 14]. The latter offers a great technical and economic potential for the fabrication of electronic and sensor devices by direct writing on the target substrate.

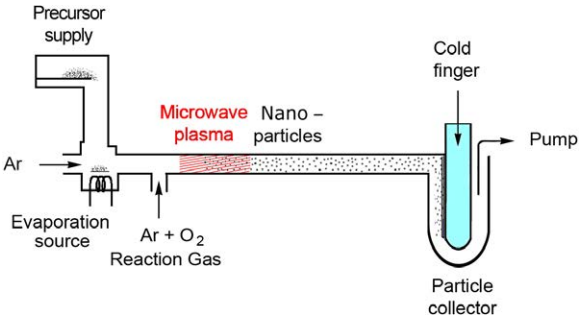

Figure 1. Microwave plasma synthesis of n-WO_3 (schematically). (This figure is in colour only in the electronic version)

Tungsten oxide is well known for its polymorphic structural and semiconductor behaviour, which depend both on the grain size and on deviations from oxygen stoichiometry. At ambient conditions, stoichiometric bulk WO_3 possesses a monoclinic lattice structure, which transforms with increasing temperature first to an orthorhombic phase at 330 °C and then above 740 °C to a tetragonal lattice structure [4, 15]. As observed for other transition metal oxides, e.g. ZrO_2 [16], the high temperature phases can be stabilized down to ambient temperature by a small grain size.

An important property of WO_3 is its n-type semiconducting behaviour, which is due to oxygen vacancies acting as shallow donor sites [17–19]. Similarly as with other transition metal oxides, e.g. SnO_2, tungsten readily assumes a lower valence, e.g. W^{4+} instead of W^{6+} [4, 5]. This process involves surface reactions that remove oxygen from the lattice and thus induce oxygen vacancies in order to maintain charge neutrality [9]. Electrons from the ionization of oxygen vacancies and the hopping between W^{5+} and W^{6+} ions contribute to the electric conductivity in WO_3 [19]. Changes in oxygen stoichiometry also determine the response of WO_3 to ambient gases by varying its electrical conductivity. Surface reactions with reducing and oxidizing gases (e.g. H_2S or O_2) induce the formation and annihilation of oxygen vacancies associated with the transfer of electrons to or from the absorbed gas molecules [18, 20, 21].

In the present work, the response of the electrical conductivity of n-WO_3 to H_2S in air is studied as a model system for a reducing gas. The present study focuses on structural and electrical conduction properties of nanoparticulate WO_3 as a function of the processing and annealing conditions. For this purpose, nanoparticulate films with a well-defined small crystallite size of about $d \sim 5$ nm are fabricated using microwave plasma synthesis. In this model system, the electrical conduction behaviour and its response to ambient gases are expected to be dominated by the high fraction of atoms at interfaces and the large specific surface of the nanoparticles.

2. Experimental procedure

Tungsten oxide nanoparticles were prepared by the method of microwave plasma synthesis [11]. Figure 1 shows a schematic drawing of the experimental set-up. In the present work $W(CO)_6$ with 99.9% purity (purchased from Sigma Aldrich) was used as a precursor with good handling properties and low toxicity. By means of a vibrating spoon, the $W(CO)_6$ powder was fed to the evaporation source. At a gas pressure of 10 mbar, $W(CO)_6$ sublimates at a temperature of about 150 °C. Pure (5N) Ar (0.4 std. l min^{-1}) carries the $W(CO)_6$ vapour to the reaction zone, where it is mixed with a reaction gas (80 vol% Ar and 20 vol% O_2, flow rate: 3–4 std. l min^{-1}) and decomposed in a microwave-induced plasma (2.45 GHz, 300 W). The WO_3 particles form in the gas stream inside the plasma zone and are subsequently collected *in situ* on a water-cooled glass finger by means of thermophoresis (figure 1). In a typical 30 min run, 1–2 g of $W(CO)_6$ is evaporated and 200–300 mg of nanoparticle powder is obtained. The n-WO_3 powder is scraped off with a razor blade and ultrasonically dispersed in isopropanol (20 mg cm^{-3}) for further processing [22]. The XRD measurements were performed using a Bruker diffractometer D8 Advance using a θ–2θ geometry and Cu Kα radiation. For transmission electron microscopy, the n-WO_3 powders were ultrasonically re-dispersed in ethanol and a small quantity deposited on a carbon film. All TEM micrographs were taken with a Philips CM20 microscope (see figure 2).

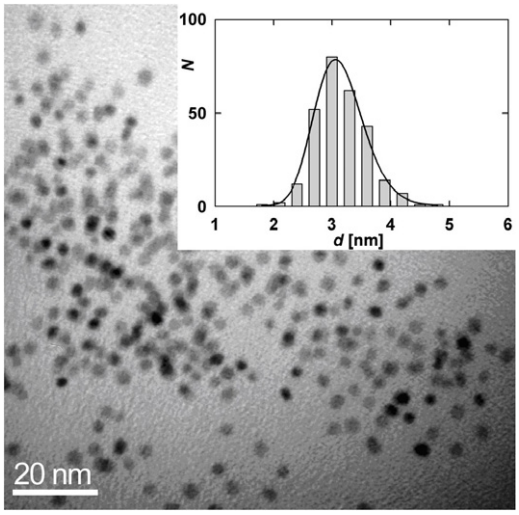

Figure 2. (left) TEM micrograph of tungsten oxide nanoparticles ultrasonically re-dispersed in 2-propanol. The inset shows the size distribution of the particle diameter d with a log-normal function fitted.

For the conductivity measurements a test device with four interdigital Au electrodes on a glass substrate is prepared by photolithography using a contact mask of 0.2 mm structural width [22]. The contact electrodes were made by depositing layers of Cr (10 nm) and Au (50 nm) in high vacuum. Within an area of 1 cm^2, the device comprised four parallel electrodes with an effective length of 10 cm for the resistance measurements. Homogeneous films of tungsten oxide nanoparticles with typical thicknesses of 10 μm were deposited on the device by repeated (20×) spin-coating with a dispersion of 1 g l^{-1} n-WO_3 in 2-propanol.

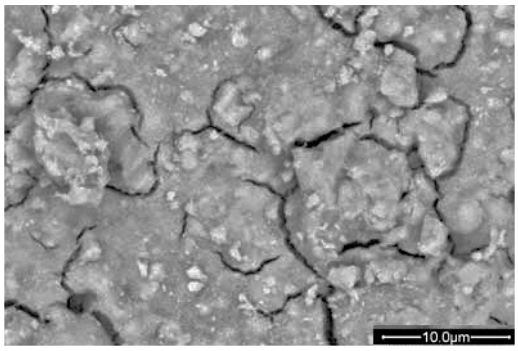

Figure 3. Backscattered electron micrograph of nanoparticulate WO_3 film after spin-coating on a glass substrate and annealing in air at 500 °C.

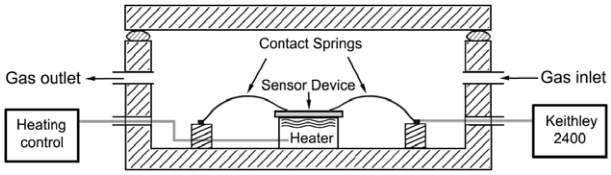

Figure 4. Measurement cell for testing the response of n-WO_3 to gases. Gold-plated springs contact the n-WO_3 film. The electrical resistance is measured with a Keithley 2400 sourcemeter.

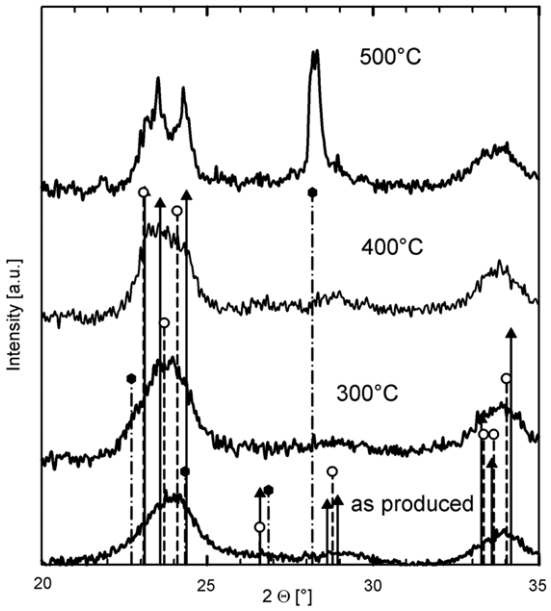

Figure 5. X-ray diffraction of a nanoparticulate tungsten oxide film deposited on a glass substrate before and after annealing at the quoted temperatures for 8 h. The positions and relative intensities of the Bragg reflections of monoclinic (▲), orthorhombic (⭘) and hexagonal (⬢) WO_3 are indicated.

The deposited tungsten oxide layer was pre-annealed in air at temperatures between 300 and 500 °C (typically 8 h) in order to equilibrate the oxygen stoichiometry and to stabilize the film structure for the subsequent measurements. The n-WO_3 films were examined by x-ray diffraction after each annealing step (figure 5).

In addition, the film structure of identically processed specimens was studied by means of environmental scanning electron microscopy using an FEI Quanta 600 instrument in a humid atmosphere of 0.5 mbar at 15 kV. Thereby, ESEM micrographs could be recorded without applying an extra conductive layer, e.g. of Au. Backscattered electron (BSE) micrographs show that the films are continuous and at least 1 μm thick. Therefore, the underlying gold conductors do not show up in the Z-sensitive BSE images (figure 3) or in accompanying studies using energy dispersive x-ray analysis.

Measurements of the electrical resistance and its response to gases were performed in a vacuum-tight thermostated cell (see figure 4). The test device was placed on a ceramic heater plate with built-in Pt thermocouple and electrically contacted on the edges by gilded steel springs. The electrical conductivity was measured using the four-point method [23] and a Keithley 2400 Sourcemeter. For most of the measurements a fixed current of 10 nA was applied. Measurement control and data collection were performed with Labview software.

In view of the pre-annealing treatments and the high electrical resistance at low temperatures, measurements of the electrical conductivity and its variation due to gas exposure were generally conducted in the temperature range from 150 to 270 °C. Gas flow rates ranging from 10 $cm^3\ min^{-1}$ (H_2S in air) to 100 $cm^3\ min^{-1}$ (N_2/O_2) and the mixing ratio of the analyte gases were adjusted with mechanical flow meters made by Krohne and monitored using a bubbler. These rather low flow rates were chosen to avoid the formation of a temperature gradient over the sensor device. All gas response tests were repeated several times and on different device samples in order to confirm the reproducibility of our results.

3. Experimental results

For the tungsten oxide nanoparticles, in the state as prepared by microwave plasma synthesis, a small particle size of about 3 nm is observed by transmission electron microscopy (TEM) and x-ray diffraction (XRD) studies (figures 2 and 5). The TEM micrographs also show a narrow size distribution. More than 90% of the WO_3 particles exhibit a size between 3 and 4 nm, as well as a high degree of dispersion. Fitting a log-normal distribution to the size histogram (inset of figure 2), a mean particle diameter of 3.2 ± 0.4 nm is determined. Small agglomerates about 50 nm in size which formed during synthesis (not shown) could be broken up by ultrasonic treatment in 2-propanol.

The XRD data of nanoparticulate WO_3 (see figure 5 and table 1) are marked by broad diffraction maxima. On the one hand, this clearly demonstrates the small crystallite size. On the other hand, this may indicate a significant fraction of amorphous WO_3, especially in state as produced. Based on literature data, a mixed structure of monoclinic WO_3 with some tetragonal or amorphous WO_3 can be attributed to the WO_3 nanoparticles in the state after spin-coating and annealing at 300 °C [24, 25].

Figure 5 also indicates that additional annealing at 400 °C induces a partial transformation to orthorhombic WO_3,

Table 1. Structural properties of WO_3 in different states of processing and annealing: except for bulk WO_3 in thermal equilibrium, the data refer to measurements at ambient conditions after annealing at the listed temperatures. m, t, o and h denote monoclinic, tetragonal, orthorhombic and hexagonal lattice structure of WO_3, respectively. Grain sizes and temperatures are given in brackets.

Processing and annealing	Spin-coated on glass (this work)	Bulk in thermal equilibrium (a)	Pulsed-laser deposition on glass (b)	Reactive deposition on Al_2O_3 (c)	PVDWO_3 on Al_2O_3 in humid air (d)
RT/as-produced	m, partly amorphous	m (RT—340 °C)	Amorphous	m + t (10 nm)	m (3 nm)
300 °C	Mainly m (<10 nm)	m	m (XRD, AFM)	m + t (10 nm)	o (150 °C)
400 °C	m, o	o (330–740 °C)	o	m + t	h (300 °C)
500 °C	h (∼20 nm)	o	h	m + some t	Magnéli—$WO_{2.9}$
⩾550 °C	m	o, (>740 °C): t		100% m (600 °C) (40 nm)	

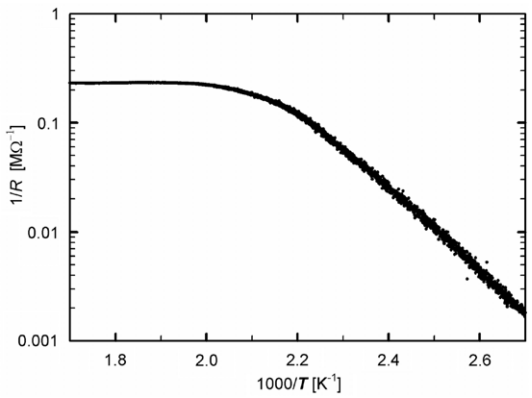

Figure 6. Variation of the conductance $1/R$ of a nanoparticulate WO_3 film with temperature T. From the fit of an Arrhenius-type behaviour in the range 100–200 °C an activation energy of 0.31 eV is deduced.

probably accompanied by a slight crystallite growth. Further annealing at 500 °C induces profound structural change, as a transformation to hexagonal WO_3 is accompanied by significant grain growth. Based on the Scherrer equation [26] a crystallite size d of 25 ± 5 nm is estimated for n-WO_3 annealed at 500 °C. In TEM studies on n-WO_3 powder samples with identical annealing treatment an average crystallite size of the order of 20 nm with some larger grains up to 50 nm in size was observed.

The variation of the electrical resistance of WO_3 with temperature T is shown in figure 6. Measurements were performed in dry synthetic air after pre-annealing at 400 °C. A reversible decrease of the resistance by more than two orders of magnitude with increasing temperature from 100 to 200 °C is observed, typical for a semiconductor. From this temperature dependence, the activation energy of 0.31 eV is deduced for the charge carrier conduction. In the subsequent temperature range up to 330 °C the electrical conductivity remains almost constant (see figure 6).

The effect of the oxygen partial pressure on the electrical resistance of the n-WO_3 films is shown in figure 7. Upon cycling with pure varying O_2-admixtures in N_2, a fully reversible increase of the electric resistance by up to 50% is observed (figure 7(a)). The largest variation is observed for the step from 0 to 1.1 vol% O_2 in N_2, as the increase of $\Delta R/R$ becomes smaller at higher O_2 concentrations, indicating a saturation effect (figure 7(b)). The relative resistance variation with the O_2 content is significantly enhanced at the higher measuring temperature of 250 °C (figure 7(b)). Measurements of the response time for obtaining 90% of the total resistance variation for exposure to 1.1% O_2 in N_2 show a decrease from 10 min at 200 °C to 3 min at 270 °C, as expected for a thermally activated process.

The variation of the electrical resistance of WO_3 upon a stepwise change from 0 to 10 ppm of the H_2S concentration in air is shown in figure 8(a). These measurements were performed at an operational temperature of 200 °C after pre-annealing at 300 °C. A change of the resistance is already noticeable for H_2S levels as low as 1 ppm. Exposure to 10 ppm H_2S leads to a drop of the resistance by about 80%.

The effect of the measuring temperature on the response to 10 ppm H_2S is presented in figure 8(b). After pre-annealing at 300 °C, the largest response to H_2S ($\Delta R/R \sim 0.5$) was observed at the lowest operational temperature of 150 °C (figure 8(b)). For increased operational temperatures of 175 and 200 °C, a decrease of the total resistance R and the relative variation ($\Delta R/R$) upon exposure to H_2S was observed. The response of the n-WO_3 films to 10 ppm H_2S was fully reversible, although a slight hysteresis between the variation of the electrical resistance upon increasing and decreasing concentrations of H_2S was noted (see figures 8(a) and (b)). Within the concentration range studied, the electrical conductivity of n-WO_3 shows a nearly linear response to the concentration of H_2S in air.

The effect of different pre-annealing treatments on the response to H_2S is shown in figure 8(c). All measurements were performed at an operating temperature of 150 °C with cyclic exposure to pure synthetic air and 10 ppm of H_2S in air. Specimens pre-annealed only at 300 °C show the largest resistance variation and the shortest response time. Subsequent pre-annealing at 400 °C leads to a small decrease of the electrical resistance in synthetic air and a larger reduction of the response to H_2S. Further pre-annealing at 500 °C leads to a marked increase of the electrical resistance and a corresponding reduction of the relative response $\Delta R/R$ to H_2S. It is interesting to note that x-ray diffraction (figure 5) shows a transformation to hexagonal WO_3 in this state of annealing.

4. Discussion

The assessment of the structural evolution of nanoscale WO_3 as a function of processing steps and annealing treatments

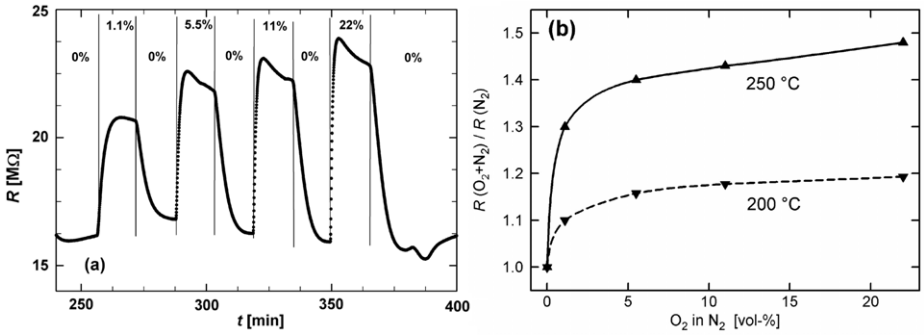

Figure 7. (a) Time dependence of the electrical resistance R of n-WO_3 measured at 250 °C upon cycling with pure N_2 and admixtures with O_2 (vol-%), as indicated. (b) Relative variation $\Delta R/R$ of the resistance with oxygen concentration for operating temperatures of 200 and 250 °C.

constitutes an important part of the present study. The x-ray diffraction data (see figure 5) indicate that annealing at 300 °C in air does not induce significant grain growth, but apparently does promote crystallization of the initially—at least in part—amorphous tungsten trioxide nanoparticles. After subsequent deposition by spin-coating, a structure of mainly monoclinic WO_3 with a small crystallite size ($d < 10$ nm) is observed (see table 1, compare as-produced and 300 °C). Similarly, the retention of the originally prepared structure of monoclinic or partly tetragonal WO_3 in this temperature range is generally reported in the literature (see table 1). A comparison of these studies (see table 1) shows no significant effect of the synthesis route or substrate on the resulting lattice structure after annealing at 300 °C [7, 9]. Only in the presence of water vapour were surface reactions observed, including a transformation first to large orthorhombic domains and—upon further heating to 300 °C—to a hexagonal structure of small grains [24].

From our XRD data (figure 5), recorded after additional annealing at 400 °C, the completion of crystallization accompanied by a partial transformation to the orthorhombic phase and slight grain growth is deduced. A similar behaviour was reported by Ramana *et al* [27] for laser-deposited WO_3 on glass, whereas Reyes *et al* [9] did not observe such a transformation in the case of WO_3 films on Al_2O_3 with a starting grain size of $d \sim 10$ nm.

In contrast to the processing steps discussed so far, additional annealing at 500 °C (8 h) did induce a major change of the structural and, as discussed below, the electrical conduction behaviour of the n-WO_3 films. As shown in the upper part of figure 5, significant grain growth to an average size of $d \sim 25$ nm is accompanied by a structural transformation to hexagonal WO_3. A comparison with literature data suggests that the formation of hexagonal WO_3 does apparently depend on the substrate used for the n-WO_3 films. It is interesting to note that hexagonal n-WO_3 was only observed on glass substrates in this work and by Ramana *et al* [27], whereas monoclinic n-WO_3 is retained on sapphire [9].

In the present work, the limited thermal stability of the test devices used precluded extended annealing at temperatures above 500 °C, for which a transformation back to a monoclinic lattice structure was observed. Based on these results, a temperature range of 150–270 °C—significantly lower than for the pre-annealing treatments—was chosen in order to maintain the n-WO_3 films stable during the measurement runs. No evidence of structural deterioration is observed in accompanying x-ray diffraction and optical microscopy studies.

Studying the electrical conductivity of n-WO_3 is a key issue of the present work, as it is closely linked with the stoichiometry and the response to ambient gases. At temperatures below 500 °C, WO_3 shows an n-type semiconducting behaviour, which is governed by the ionization of oxygen vacancies acting as shallow donor sites [17–19]. Each oxygen vacancy can donate up to two electrons to the conduction band according to

$$V_O \leftrightarrow V_O^{\cdot\cdot} + 2e^-. \tag{1}$$

An Arrhenius plot of $1/R$ over $1/T$ (figure 6) clearly indicates two temperature ranges of the electrical conductivity. In the range from about 100 to 200 °C, the conductivity of n-WO_3 shows an exponential increase with temperature, as is typical for a semiconductor, from which an activation energy of about 0.31 eV is estimated. At temperatures above 200 °C the conductivity remains almost constant; this is attributed to a complete ionization of the oxygen vacancies acting as donor sites. These findings are in agreement with the n-type semiconductor model and data in the literature for specimens with monoclinic or orthorhombic structures, for which activation energies in the range from 0.15 to 0.6 eV are reported [18, 19].

The oxygen vacancies result in part from the small energy barrier of the transition metal cations to assume lower chemical valences. Such a transition, e.g. from W^{6+} to W^{4+}, is accompanied by the formation of an oxygen vacancy in order to maintain charge neutrality [4]. Alternatively, oxygen vacancies in WO_3 can be created or annealed out by removing or adding oxygen from the surrounding atmosphere in a surface reaction which involves an exchange of electrons with the lattice [9, 20]:

$$V_O^{\cdot\cdot} + 2e^- + 1/2O_2 \leftrightarrow O_O. \tag{2}$$

Additionally, the adsorption (and desorption) of oxygen at the WO_3 surface directly contributes to removing or adding conduction electrons according to

$$O_2(\text{gas}) + e^- \leftrightarrow O_2^-(\text{adsorbed}). \tag{3}$$

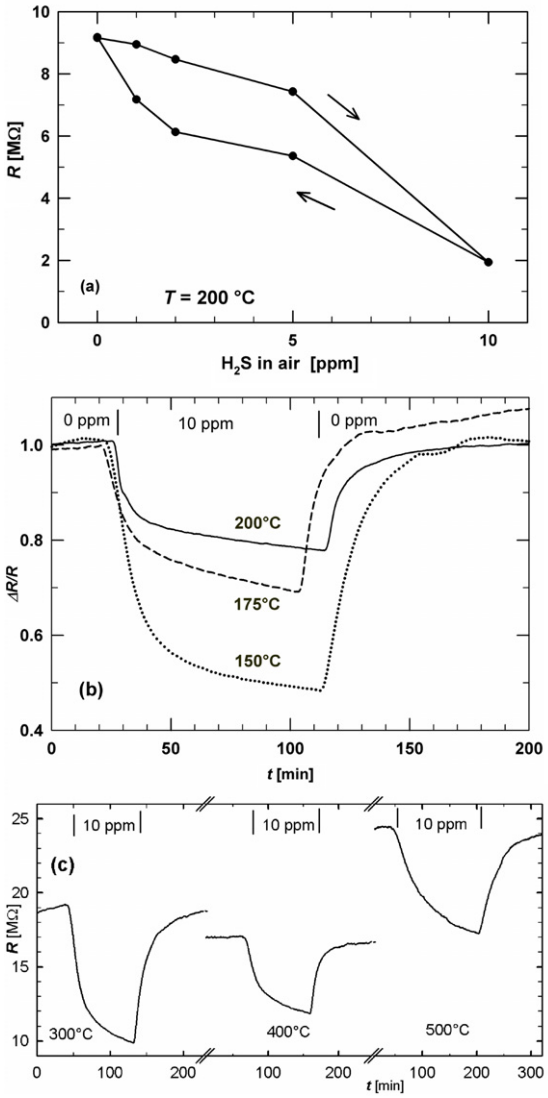

Figure 8. Variation of the electrical resistance R of an n-WO_3 film upon exposure to H_2S in synthetic air: (a) variation with concentration (vol—ppm) of H_2S measured at 200 °C after pre-annealing at 300 °C. (b) Time dependence of the resistance R for various measuring temperatures (after pre-annealing at 300 °C). (c) Time dependence of R for various pre-annealing temperatures, measured at 150 °C.

The adsorption of additional oxygen, e.g. upon rising partial pressure of O_2, therefore contributes to forming an electron-depleted surface layer of low conductivity on the WO_3 grains, see equation (3). Conversely, a reduction of the amount of adsorbed oxygen, e.g. due to exposure to pure N_2, also draws oxygen from the WO_{3-x} grains, giving rise to the formation of oxygen vacancies and W^{4+} ions. According to equation (1) this increases the amount of free electrons and hence the electrical conductivity. Based on these considerations the observed increase of R (figure 7) upon exposure to oxygen is ascribed to the oxygen uptake according to equations (2) and (3). The stronger response at 250 °C (figure 7(b)) is attributed to a thermally activated uptake of O_2 into the grains according to equation (2).

Additional annealing at 500 °C leads to a marked decrease in conductivity (see figure 8(c) right). In the context of our x-ray diffraction studies (see figure 3) this behaviour is attributed to a structural transformation to hexagonal WO_3, for which a reduced electrical conductivity and higher activation energy of 0.87 eV is reported in the literature [24].

As briefly outlined above, changes in oxygen stoichiometry also determine the response of WO_3 to other ambient gases. Surface reactions with reducing and oxidizing gases (e.g. H_2S or NO_2) induce both a formation (respectively annihilation) of oxygen vacancies and a transfer of electrons from/to the adsorbed gas molecule [9]. Oxygen adsorbed at the WO_3 surface also plays a key role in the response to H_2S in air, for which the reaction steps

$$O^-_{2(ads)} + e^- \leftrightarrow 2O^-_{(ads)} \tag{4}$$

and

$$H_2S_{(ads)} + O^-_{(ads)} \leftrightarrow H_2O + S + e^- \tag{5}$$

constitute the main reaction pathway in the temperature range studied [8]. Alternatively, sulfur may react with the grain surface according to [20]

$$3WO_3 + 7H_2S \rightarrow 3WS_2 + SO_2 + 7H_2O. \tag{6}$$

In sum, the surface reactions with H_2S remove oxygen from the n-WO_3 film, donate electrons to the conduction band and thereby enhance the electrical conductivity. Therefore a linear relation between the amount of H_2S present and the increase of the electrical conductivity is expected for low concentrations of H_2S. This behaviour was indeed observed in the present work (figure 8) and is reported in the literature for up to 100 ppm H_2S in air [9].

The variation of R with time (figures 8(a) and (b)) also shows that the response to decreasing concentrations of H_2S is slower than observed for increasing H_2S concentrations, particularly at low operational temperatures. In view of the reaction pathway given above in equations (5) and (6) this behaviour is attributed to a slow desorption of the adsorbed H_2S and the reaction products from the WO_3 surface as the rate-limiting process [9].

However, the resistance variation $\Delta R/R$ observed in the present work is smaller than generally reported in the above cited studies for the response of the electrical resistance of WO_3 to H_2S or NO_x in this temperature range. It is also interesting to note that the present results (see figure 8(c), left) are similar to the literature data for 10 nm WO_3 particles [9], whereas studies using larger particles show higher response to small concentrations of H_2S [8]. These findings suggest that both the small particle size of n-WO_3 films after pre-annealing at 300 and 400 °C and the remaining fraction of amorphous WO_3 particles may contribute to the observed smaller response to gases (see also figure 5).

This interpretation is supported by further studies in the literature which also indicate a decrease in sensitivity for small particles. Tamaki *et al* [10] studied the sensitivity of WO_3 to NO_2 as a function of the crystallite size and observed maximum sensitivity for values of d of the order of 30 nm.

In this respect, the reduction in gas-sensing potential for small particles can be well understood as it is attributed to a combined effect of grain boundaries and of space charge zones. With decreasing crystallite size the conduction behaviour becomes more and more dominated by grain boundaries and corresponding space charge zones with low conductivity that exert a detrimental effect on gas sensitivity [28, 29] since this additional resistance reduces the relative variation $\Delta R/R$ of the overall resistance attainable in contact with gases. This is especially noted at higher measuring temperatures for which good conductivity within the grains is observed (figures 6–8).

The observed reduction of the sensitivity to H_2S at higher operational temperatures, which is also reported in the literature [9, 20], may also be attributed to the complex and competing reaction pathways (equations (3)–(7)) with H_2S on the WO_3 surface, for which unfortunately no reaction enthalpy data are available. In accordance with previous reports our observations of a reduced sensitivity at higher measuring temperatures may also be attributed to the reduced contribution of a second reaction mechanism acting at lower temperatures:

$$2H_2S_{(ads)} + 3O^-_{2(ads)} \leftrightarrow 2H_2O + 2SO_2 + 3e^-, \qquad (7)$$

which donates more conduction electrons [9].

The effect of different pre-annealing and operational temperatures on the response of n-WO_3 films to 10 ppm H_2S in air is presented in figure 6(c), which clearly shows the largest response to H_2S for n-WO_3 samples pre-annealed at 300 °C, similar to that found by Reyes *et al* [9]. In accordance with the results of our structural studies, the decrease of $\Delta R/R$ and R in the second step of annealing (400 °C) may be attributed both to the crystallization of the remaining amorphous WO_3 and a decrease of the surface to grain boundary area ratio due to grain growth and the onset of sintering.

In contrast to the expectation from literature data [9, 10] annealing the n-WO_3 film at 500 °C did not enhance the conductivity and response to H_2S. As shown in figure 6(c), an overall increase of the electrical resistance and a smaller response $\Delta R/R$ to gas exposure is observed than for a specimen annealed only at 300 °C. In reference to the structural data from x-ray diffraction (see figure 3 and table 1), the drop in conductivity and sensitivity observed is attributed to the formation of hexagonal WO_3 as observed after annealing at 500 °C. This view is also supported by the literature data of hexagonal WO_3 [5, 24] reporting a higher activation energy and consequently a lower electrical conductance and response to ambient gases than of monoclinic WO_3.

Summing up the present experimental findings, it may therefore be concluded that microwave plasma synthesis is a suitable processing route for obtaining nanoparticulate WO_3 with the favourable properties of a small, uniform particle size and easy dispersion in liquids. Whereas this starting material is well suited for device fabrication by spin-coating or ink-jet printing, a larger particle size is required to obtain an optimal response to gases. In view of the present results, the necessary annealing steps and the substrate must be carefully chosen in order to avoid the formation of unwanted phases, especially hexagonal WO_3.

Acknowledgments

Financial support of the Österreichische Forschungsförderungsgesellschaft FFG (Project Cluster 702 ISOTEC / SENSPHYS) is appreciated. Grateful thanks are due to DI W Reinberger, NanoTecCenter Weiz Forschungsgesellschaft GmbH, for technical advice and DI Angelika Reichmann, Institute for Electron Microscopy and Fine Structure Research, Graz University of Technology, for ESEM microscopy.

References

[1] Vollath D 2008 *Nanomaterials—An Introduction to Synthesis, Properties and Applications* (Weinheim: Wiley–VCH)
[2] Yamazoe N 1991 *Sensors Actuators* B **5** 7
[3] Göpel W and Schierbaum K D 1995 *Sensors Actuators* B **26** 1
[4] Eranna G, Joshi B C, Runthala D P and Gupta R P 2004 *Crit. Rev. Solid State Mater. Sci.* **29** 111
[5] Moulzolf S C, Ding S and Lad R J 2001 *Sensors Actuators* B **77** 375
[6] Sberveglieri G 1992 *Gas Sensors: Principles, Operation and Developments* (New York: Springer)
[7] Solis J J, Saukko S, Kish L, Granqvist C G and Lantto V 2001 *Thin Solid Films* **391** 255
[8] Jimenez I, Arbiol J, Dezeanneau G, Cornet A and Morante J R 2003 *Sensors Actuators* B **93** 475
[9] Reyes L F, Hoel A, Saukko S, Heszler P, Lanto V and Granqvist C G 2006 *Sensors Actuators* B **117** 128
[10] Tamaki J, Zhang Z, Fujimori K, Akiyama M, Harada T, Miura N and Yamazoe N 1994 *J. Electrochem. Soc.* **141** 2207
[11] Vollath D and Szabó D V 2006 *J. Nanopart. Res.* **8** 417
[12] Winterer M 2002 *Nanocrystalline Ceramics—Synthesis and Structure* (Berlin: Springer)
[13] Sagmeister M, Brossmann U, List E J W, Ochs R, Szabó D V and Würschum R 2008 *Phys. Status Solidi RRL* **2** 203
[14] Böberl M, Kovalenko M V, Gamerith S, List E J W and Wolfgang H 2007 *Adv. Mater.* **19** 3574
[15] Lassner E and Schubert W D 1999 *Tungsten—Properties, Chemistry, Technology of the Element, Alloys and Chemical Compounds* (New York: Kluwer) p 146
[16] Sagmeister M, Brossmann U, List E J W, Ochs R, Szabó D V, Saf R, Grogger W, Tchernychova E and Würschum R 2010 *J. Nanopart. Res.* **12** 2541
[17] Sawada S 1956 *J. Phys. Soc. Japan* **11** 1237
[18] Gillet M, Lemire C, Gillet E and Aguit K 2003 *Surf. Sci.* **532** 519
[19] Hutchins M G, Abu-Alkhair O, El-Nahas M M and Abdel-Hady K 2006 *J. Phys.: Condens. Matter* **18** 9987
[20] Barrett E P S, Georgiades G C and Sermon P A 1990 The mechanism of operation of WO_3-based H_2S sensors *Sensors Actuators* B **1** 116
[21] Gallardo I J 2003 Tungsten oxide nanocrystalline powders for gas sensing applications *Doctoral Thesis* University of Barcelona
[22] Sagmeister M 2009 Microwave plasma synthesis and characterization of oxide nanoparticles *Dissertation* Graz University of Technology
[23] van der Pauw L J 1958 *Phil. Res. Rep.* **13** 1
[24] Al Mohammad A 2008 *Phys. Status Solidi* a **205** 2880
[25] *PDF-2 The Powder Diffraction File Rel. 2001* (Newtown Square (PA): The International Center for Diffraction Data)
[26] Klug H P and Alexander L E 1974 *X-Ray Diffraction Procedures* (New York: Wiley) p 656
[27] Ramana C V, Utsunomiya S R, Ewing R C, Julien C M and Becker B 2006 *J. Phys. Chem.* B **110** 10430
[28] Sun H T, Cantalini C, Lozzi L, Passacantando M, Santucci S and Pelino M 1996 *Thin Solid Films* **287** 258
[29] Göpel W 1996 *Sensors Actuators* A **56** 83